Field-Supported Verification and Improvement of a Passive Microwave Surface Emission Model for Rough, Bare, and Wet Soil Surfaces by Incorporating Shadowing Effects

David N. Kuria, Toshio Koike, Hui Lu, Hiroyuki Tsutsui, and Tobias Graf

Abstract—To investigate the potential of passive microwave techniques for observing the atmosphere over land, it is important to understand the nature of emissions from the land surface. The heterogeneity of large-scale land surface emissions has been cited as a major impediment in conducting observations of the atmosphere over land. Many models, both theoretical and empirical, have been developed to explain the surface emission with varying degrees of success. In the past, most field-supported research in soil observations using microwave techniques has concentrated on lower frequencies (L-band). This paper reports on a study, supported by field data, that seeks to improve our understanding of surface emission at various frequencies using passive microwave radiometers. This provides a crucial link between remote sensing of the land surface and the atmosphere. We show that it is important to consider shadowing associated with rough wet surfaces. By incorporating shadowing effects, the advanced integral equation model (AIEM) shows remarkable agreement with observations at all frequencies and polarizations. Although the roughness parameters obtained during our experiment correspond to very rough conditions, by including shadowing effects the AIEM model is able to transition from the not so rough natural condition as observed from space to the very rough as obtained during field experiments.

Index Terms—Microwave, periodic roughness, shadowing, surface emission modeling.

I. INTRODUCTION

THE HETEROGENEITY of large-scale land surface emission has been cited as the main impediment in conducting observations of the atmosphere over land using passive microwave techniques [11], [23]. This emission is dependent on the nature of the soil surface, i.e., the amount of soil moisture and the roughness of the surface. If the roughness condition of the surface is ignored, the retrieved soil moisture condition underestimates the actual soil moisture condition. Under dry conditions, emission from deeper soil layers attenuated by volume scattering is dominant; however, for soil containing considerable moisture, emission from the deeper layers is masked

out, and in this case, emission from the soil surface dominates. Though emissions from bare soil surface are well understood theoretically, it has not been adequately explained from field experiment data. This is especially true at higher microwave frequencies, as such data are lacking, and this severely limits the quality of atmospheric information that is retrievable over land. To compound the issue, most previous field studies carried out within this framework have been restricted to the L-band range, neglecting the higher frequencies that carry substantial information on the overlying atmosphere. Surface emission is thus doubly important because it serves as the lower boundary for upwelling radiation from the soil to the atmosphere and the upper boundary for downwelling radiation from the atmosphere into the soil volume.

The scattering of microwave signals emitted by a medium or incident on a medium with a rough surface boundary has been studied extensively for many years [17]. Accordingly, many scattering and emission models have been developed, both physical and empirical. However, most of these previous studies have been conducted within active microwave remote-sensing applications. In passive microwave cases, the empirical model in [6] is widely used to model emission accounting for surface scattering due to the roughness of the surface. Among the physically based models, the advanced integral equation model (AIEM) is best suited to describe surface emission and surface scattering for a broad range of surface roughness conditions and frequencies.

The sensitivity of a microwave signal to surface roughness is well known qualitatively, but poorly understood quantitatively, especially under natural field conditions [14]. In the case of radar sensing, the dynamic range of the backscattering coefficient associated with surface roughness is comparable to or larger than that associated with soil moisture. For this reason, surface roughness must be estimated accurately to ensure that soil moisture is retrieved accurately [12]. Another key factor that should be addressed in surface emission models is the effect of shadowing. On the basis of conventional theories of surface scattering, it is normally assumed that every point on the surface contributes to the scattered or emitted wave, including points in the shadowed region. This assumption neglects shadowing of the surface by the surface itself, an effect that is especially important at large angles of incidence [2].

Accordingly, the objectives of this paper are to report on: 1) field-data-supported selection and verification of an

appropriate physically based surface emission model for application in multifrequency microwave remote sensing; 2) the benefits of incorporating the effects of shadowing within the surface emission model; and 3) the generation of a comprehensive brightness-temperature observations data set under varying conditions of soil moisture and surface roughness.

The organization of this paper is given as follows. In Section II, we first present an overview of surface scattering and emission theory in which we review selected surface emission models and shadowing theory in Section II-A and B. We then present an overview of the field experiments conducted to clarify the effects of surface roughness in Section III. The performance of the selected models is presented in Section IV. We present the results of observations obtained with a soil moisture content of 15%, as emissions from the metal background are masked out. We also present an analysis of the effects of shadowing and the influence of soil moisture on shadowing. Finally, we present the model validation and conclusions arising from our experiments and simulations in Sections V and VI, respectively.

II. SURFACE SCATTERING AND EMISSION THEORY

A. Surface Emission Models

When an electromagnetic wave impinges upon a boundary surface between two semi-infinite media, a portion of the incident energy is scattered and the rest is transmitted. This scattering at the surface is mainly dependent on the dielectric constants of the media and the condition of the boundary surface, i.e., the surface roughness of the boundary interface. The condition of the boundary surface also determines those points on the surface that will be in shadow and those that will be illuminated, depending on the incidence angle of the impinging (active) or emergent (passive) radiation.

A surface emission model is an essential component in many applications of microwave remote sensing of the geophysical properties of terrain upon earth. The various applications of surface emission models are outlined by Shi *et al.* [15]. There are two main approaches that are in common usage in surface emission modeling, namely: 1) physical modeling and 2) semiempirical approaches. Semiempirical approaches are easy to use and are especially recommended for image-based (grid-based) data analyses. Shi *et al.* [15] outlined the limitations of semiempirical surface emission models that are currently in use. A key limitation of semiempirical models is their restricted scope of applicability (frequency range, roughness condition, etc.). A number of semiempirical models are able to match field measurements with a reasonable degree of accuracy [10], [22]. Depending on the range of experimental data, these models can work reasonably well, but only within a particular setting. The majority of these models were developed for low-frequency measurements (L-band). Of the semiempirical models, the QH model is the most commonly used; it describes bare surface emission as a function of surface roughness and dielectric properties, i.e.,

$$R_p = [Q \cdot r_p + (1 - Q) \cdot r_q] \cdot H \qquad (1)$$

where q and p refer to the polarization states v and h, respectively, and r is the Fresnel reflectivity. The roughness parameter Q describes the energy emitted in orthogonal polarization due to roughness effect. The parameter H describes the effect of surface roughness on reducing the surface effective reflectivity with increasing frequency. These parameters are given as [20]

$$Q = 0.35 \cdot (1 - e^{-0.6\sigma^2 f}) \qquad (2)$$

$$H = e^{-(2 \cdot k\sigma \cos \theta)^2} \qquad (3)$$

where f is the frequency in gigahertz, k is the wavenumber, θ is the angle of incidence, and σ is the root-mean-square (rms) height. The simulated surface reflectivity (emissivity) decreases (increases) excessively as $k\sigma$ increases; consequently, the model cannot be used at higher frequencies. The parameters Q and H are determined empirically from experimental data. This model was initially considered as a candidate surface emission model, but was dropped from consideration because it: 1) is an empirical model with no physics-based theoretical background; 2) makes the assumption that the correlation length of a surface has no effect on surface emission; 3) has a limited range of applicability for a given set of parameters; and 4) is poorly suited for higher frequencies.

For theoretical models, surface effective reflectivity R_p^e consists of the following two components: 1) a coherent component R_p^{coh} and 2) a noncoherent component R_p^{non}, which can be obtained by hemispherical integration of the bistatic scattering coefficient over the upper medium, i.e.,

$$
\begin{aligned}
R_p^e &= R_p^{\mathrm{coh}} + R_p^{\mathrm{non}} \\
&= r_p \cdot \exp\left[-(2 \cdot k\sigma \cdot \cos\theta)^2\right] + \frac{1}{4\pi \cos\theta} \\
&\quad \times \int_0^{2\pi}\int_0^{\pi/2} [\sigma_{pp}(\theta, \theta_j, \phi_j) + \sigma_{pq}(\theta, \theta_j, \phi_j)] \\
&\quad \times \sin\theta_j \cdot d\theta_j \cdot d\phi_j
\end{aligned}
\qquad (4)
$$

where q and p refer to the polarization states v and h, respectively, j is the scattering direction, r is the Fresnel reflectivity, k is the wavenumber, and σ is the rms height.

Among the physically based models, the integral equation model (IEM) has a much wider application range of surface roughness conditions than that of conventional models, such as the small perturbation model, physical optics model, geometric optics model [8], and Kirchhoff's approximation. The IEM has been further extended to the AIEM [5]. Compared with simulation data derived from the Monte Carlo model, AIEM shows a significant improvement in prediction accuracy. The main limitation of the AIEM is its complexity. Use of the model in retrieving geophysical parameters from microwave radiometer data is difficult because the model is computationally intensive. To address this limitation, Shi *et al.* [15] developed a parameterized surface emission model (the QP model) for frequencies of the Advanced Microwave Scanning Radiometer
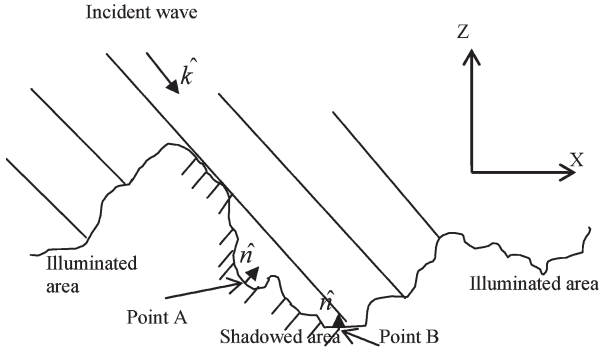
Fig. 1. Geometry of the shadowing problem.

housed aboard the Earth Observing Satellite (AMSR-E). The model equations are as follows:

$$R_p = Q_p r_q + (1 - Q_p) r_p \tag{5}$$

$$\log\left(Q_p(f)\right) = a_p(f) + b_p(f) \log\left(\frac{s}{L}\right) + c_p(f)\left(\frac{s}{L}\right) \tag{6}$$

$$Q_p(f) = d_p(f) + e_p(f) Q_p(10.65) \tag{7}$$

where r_p and r_q are the Fresnel reflectivities, Q_p and Q_q (the Q parameter that corresponds with p and q, respectively) are as described above, s is the rms height, L is the correlation length, and a–e are the frequency- and polarization-dependent parameters. These two models were short-listed as candidate surface-emission models because of the advantages that they possess, i.e., being physically based and having wide application ranges in terms of both frequency and roughness conditions.

For a nadir-looking radiometer, the aforementioned description represents the theoretical treatment of roughness and its effect on surface emissions. For nonnadir observations, the effects of geometric self-shadowing due to surface roughness need to be considered. Section II-B outlines the theoretical treatment of the shadowing problem.

B. Shadowing

Consider the case of a wave impinging on a rough surface (Fig. 1) at an angle θ. When the angle of incidence is not normal to the x–y plane, a number of points on the rough surface are not directly illuminated. For some points, the local angle of incidence θ_l is not defined because

$$\cos\theta_l = -\hat{n} \cdot \hat{k}_i < 0 \tag{8}$$

where n is the surface normal at each point, and k is the incident wave vector.

All points on the rough surface with local slopes such as those shown in Fig. 1 are not illuminated directly. A number of other points are not directly illuminated even though the local angle of incidence is well defined. This occurs because of the height of the rough surface at the relevant point relative to the heights of surrounding points. The phenomenon of shadowing therefore reduces the reflectivity of the rough surface via redirection of the signal that is reflected into the shadowed area. This apparent loss translates into an increase in the emissivity of the rough surface if the laws regarding the conservation of

energy are to hold. For near-normal angles of incidence, there is little shadowing and most of the rough surface is illuminated. As the incidence angle increases, however, the shadowing effect dominates. In this paper, we used an incidence angle of $55°$ for the AMSR sensor. In our case, therefore, shadowing is significant and cannot be ignored.

The findings of previous studies on shadowing effects are summarized in [17]. Shadowing effects have been considered in microwave remote sensing over ocean surfaces [4], [8], in a limited number of active microwave applications over land surfaces [17], and in applications within the visible range of the electromagnetic spectrum [1]. Bourlier and Berginc [3] review efforts to incorporate shadowing effects into theoretical formulations in addressing the problem of the scattering of electromagnetic waves from a randomly rough surface. Failure to account for the effects of surface self-shadowing that occur in the illumination of these surfaces is reported to be the reason for the failure of theoretical models in estimating the scattering coefficient and emissivity. The majority of previous studies are limited to theoretical treatments of shadowing without supporting field data.

The problem of geometric self-shadowing on a randomly irregular surface is a difficult one, and solutions of varying degrees of complexity have been proposed [9]. The following shadowing functions proposed in [13] and [16] are adopted for this paper because they are simple yet reasonably representative:

$$S(\theta_s, \theta_i) = \begin{cases} \frac{1}{1+\Lambda(\mu_s)}, & \theta_s \geq \theta_i \\ \frac{1}{1+\Lambda(\mu_i)}, & \theta_s \leq \theta_i \\ \frac{1}{\Lambda(\mu_s)+\Lambda(\mu_i)+1}, & \text{otherwise} \end{cases} \tag{9}$$

where $\mu = \cot\theta$ and

$$\Lambda(\mu) = \frac{1}{2}\left[\sqrt{\frac{2}{\pi}}\frac{s}{\mu}e^{-\mu^2/2s^2} - \text{erfc}\left(\frac{\mu}{\sqrt{2}s}\right)\right] \tag{10}$$

with s as the mean square surface slope and erfc as the associated error function. The Gaussian surface slope is also considered in this paper and is given as

$$s^2 = 2\frac{\sigma^2}{l^2} \tag{11}$$

with σ being the rms height and l being the correlation length of the rough surface.

Bruce [1] proposed a detailed approach to determine the validity range of the employed shadowing function with an emphasis on the visible light spectrum, although these ideas can be extended to the microwave range. According to his criteria, the effect of shadowing is negligible for single scattered or emitted waves when

$$\frac{\tan(90 - \theta_i)}{\tan(90 - \theta_i) + \tan(\sigma/\rho)} \geq 1.5(k\rho)^{-1/3} \tag{12}$$

where θ_i is the incidence angle, σ is the rms height, k is the wavenumber, and ρ is the correlation length.

Incorporating the shadowing function, (4) becomes

$$R_p^e = r_p \cdot \exp\left[-(2 \cdot k\sigma \cdot \cos\theta)^2\right] \cdot S(\theta,\theta) + \frac{1}{4\pi \cos\theta}$$

$$\times \int\limits_0^{2\pi} \int\limits_0^{\pi/2} [\sigma_{pp}(\theta,\theta_j,\phi_j) \cdot S(\theta,\theta_j)$$

$$+ \sigma_{pq}(\theta,\theta_j,\phi_j) \cdot S(\theta,\theta_j)] \sin\theta_j \cdot d\theta_j \cdot d\phi_j \quad (13)$$

where $S(\theta,\theta)$ and $S(\theta,\theta_j)$ are as defined in (9).

The noncoherent part of (13) is then numerically solved in AIEM using the discrete ordinate method. The four-stream solution was found to be sufficiently accurate, while improving the overall computation performance, in comparison to eight-, 16-, and 32-stream solutions.

The AIEM has three correlation functions available. For this paper, we used the Gaussian correlation function, which is defined as

$$W(\theta) = \frac{(kl)^2 e^{-(kl \sin\theta)^2}}{2}. \quad (14)$$

III. EXPERIMENT

To investigate surface roughness effects on surface emission at multiple frequencies, we designed a controlled field experiment. The field site is in the Field Production Science Center (FPSC), Graduate School of Agricultural and Life Sciences, University of Tokyo. The target footprint was 3.4 m × 5.3 m and was set out such that all channel footprints were contained in this footprint, and there was enough room left for a wooden frame to hold the target material in place. We leveled the surface as best as we could before putting the metal plates. We would then put the sand on top of these metal plates and held it in place using the wooden frame. Due to the intensity of the labor involved in moving and collecting the sand against the resources to move and collect it, we limited the depth of the sand on metal plates to 3.5 cm. To regulate the moisture content in the sand, we mixed predetermined amounts of water to the sand in a mixing equipment.

To observe brightness temperatures, we used a two-system ground-based microwave radiometer (GBMR). This two-system GBMR configuration comprised a six-channel GBMR and a seven-channel GMBR that covers the frequency ranges of 6.925, 10.65, 18.7, 23.8, 36.5, and 89 GHz at both vertical and horizontal polarizations (23.8 GHz had only vertical polarization). Fig. 2 shows the two-system observation setup. Both GBMRs contain 18.7 GHz horizontally and vertically polarized channels. Each of the GBMRs was calibrated once or twice per week before observations using an external liquid nitrogen cold load and an internal ambient hot load.

Soil moisture measurement was done using the following two methods: 1) by soil moisture and temperature measurement system (SMTMS) and 2) by can samples. From the can samples, we additionally obtained the bulk density of the sand. Soil surface temperature was measured using the SMTMS

Fig. 2.   Setup of the field experiment.

TABLE I
PENETRATION DEPTHS AT VARYING MOISTURE
CONDITIONS (IN CENTIMETERS)

Moisture (%)	6.925 GHz	10.65 GHz	18.7 GHz	23.8 GHz	36.5 GHz
1	16.6	8.6	4.5	3.7	2.8
5	3.6	1.9	1.0	0.8	0.6
10	2.0	1.0	0.5	0.4	0.3
15	1.3	0.7	0.4	0.3	0.2
20	1.0	0.5	0.3	0.2	0.2

and infrared temperature sensor. Surface roughness was also obtained by two approaches, namely: 1) by using a pin profile meter and 2) by paint method. Photos of the paint and pin profile meter impressions were taken for each roughness observation. For a given roughness condition, we made an ensemble of photographs. These photos were processed to extract the surface roughness parameters. The ensemble mean of the roughness parameters was subsequently used in our analysis section.

We use the metal plate to cut out emission from the deeper layers since it forms a high-reflective background. For very dry cases and very low moisture conditions, the penetration depth is large, but as moisture increases the penetration depth decreases. Table I shows the variation of penetration depth with increase in moisture for sand. We use the following expression to obtain the penetration depths:

$$p = \frac{3\lambda}{2\pi \cos\theta} \frac{\sqrt{\varepsilon_r}}{\varepsilon_i}. \quad (15)$$

At 15% moisture content, the emission from deeper sand layers (above the metal plate) and the cold metal background are significantly masked out. Moreover, the effect of emission and scattering within the sand volume is very small at this moisture condition due to the shallow penetration depth. We therefore chose data obtained at this moisture content for our analysis part and assume that scattering within the sand volume is insignificant.

In the field, it is difficult to make truly random rough surfaces, and as a first step therefore, some rough surfaces were made, and observations of these surfaces were carried out. We used a rake-like structure to generate the desired roughness conditions on the sand target. The intention in our experiment was to generate random roughness. Due to the limitation of

Fig. 3.   Generation of a 4-cm roughness pattern using the roughness tool.

TABLE II
EXPERIMENT CONDITIONS

Observable quantity	Value
Soil moisture	15%
Bulk density	1.224 g/cm3
Sand mean diameter	0.8 mm
Observation angle	55°
Sand; Clay	1.0; 0.0

resources and time, we used the tool to generate the rough surface. The periodicity introduced by this tool was incidental and not the object of our experiment. Roughness patterns (Fig. 3) were made using different roughness parameters (rms height and correlation length).

In summary, observation steps on a typical day were given as follows:

1) Set up metal plate on footprint.
2) Set up SMTMS (and calibrate GBMR if necessary).
3) Observe metal plate.
4) Add water to the sand up to the desired moisture conditions.
5) Put sand ($\sim$4-cm depth) on metal plates.
6) Take sand samples.
7) Observe "smooth" condition.
   a) Observe brightness temperature.
   b) Take temperature measurement.
   c) Take roughness condition (pin profile meter, paint).
8) Make roughness pattern.
9) Observe rough condition.
   a) Observe brightness temperature.
   b) Take temperature measurement.
   c) Take roughness condition (pin profile meter, paint).
10) Repeat steps 7) and 8) for different desired roughness conditions.
11) Take sand samples.
12) Collect sand and close down (SMTMS and GBMR).

For each brightness observation set, we included a sky looking observation at 35° elevation to cater for atmospheric effect removal using (14) in emissivity calculation.

Table II shows the various settings and conditions of the target.

Table III shows the observations obtained for 15% moisture condition.

TABLE III
RAW OBSERVATION DATA AT 15% MOISTURE CONDITION

Target	6v	6h	10v	10h	18v	18h	23v	36v	36h	T_g	σ (cm)	ρ(cm)
smooth	263.9	189.0	267.6	201.5	268.5	222.1	272.0	272.9	238.6	278.6	0.085	0.15
Sky	7.6	6.8	7.8	8.9	15.5	15.5	23.3	25.3	28.7	-	-	-
rough	258.3	234.7	261.8	247.0	264.3	254.7	265.9	268.4	257.6	275.6	0.53	0.82
Sky	8.3	7.6	7.9	9.0	15.6	15.8	23.6	25.4	29.3	-	-	-

IV. RESULTS AND DISCUSSION

A. Results of the Field Experiment

Brightness temperatures obtained from the field experiment were converted to apparent (effective) emissivity using the relationship

$$T_b = e \cdot T_g + r \cdot T_{\text{sky}} \qquad (16)$$

where e is the emissivity, r is the reflectivity of the surface, T_g is the physical temperature of the surface, and T_{sky} is the downwelling sky brightness temperature. From (16), we have

$$e = \frac{T_b - T_{\text{sky}}}{T_g - T_{\text{sky}}}$$

which we used to calculate the observed emissivity.

The Dobson model [7] and the Wang–Schmugge [21] model are the dielectric models commonly used in theoretical calculations of the dielectric constant. The Dobson model is used in this paper to model the dielectric constant of the sand target, with the Debye relaxation model used in the calculation of the dielectric constant of water.

To achieve simplicity while retaining clarity, the following conventions are followed in representing the employed frequency channels: 1) the 6.925-, 10.65-, 18.7-, 23.8-, and 36.5-GHz frequencies are abbreviated as 6, 10, 18, 23, and 36, respectively; 2) h or v indicates the polarization of the channel with h being horizontally polarized and v being vertically polarized; and 3) Sm and Rg indicate smooth and rough cases, respectively.

Fig. 4 shows a comparison of observation and simulation data (QH model) for both the smooth surface (left) and for the rough surface (right). For the smooth surface, we note an apparent agreement between the data sets at 36.5 GHz. There are discrepancies at lower frequencies, with the degree of discrepancy decreasing with increasing frequency. The model generally underestimates values for the smooth surface. For observations of the rough surface, however, there is improved agreement at lower frequencies, although the model is ineffective for frequencies above 10 GHz. In past studies, this model was used mainly for frequencies below 10 GHz, and we conclude that it is not suited for applications at higher frequencies in its present form. We therefore excluded this model from subsequent analyses.

Fig. 5 demonstrates the results of using QP and AIEM to model the same observations as those presented in Fig. 4. It is clear that both QP and AIEM underestimate the observed apparent emissivities, even for the smooth surface; nevertheless, both models capture the trend more consistently than the QH model. From observational data, it is apparent that increasing roughness results in a large increase in horizontally polarized
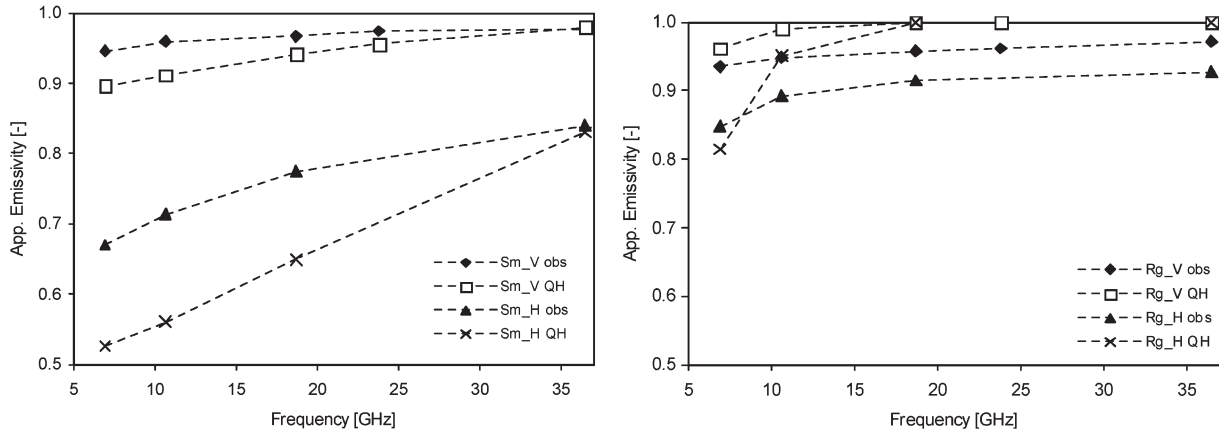
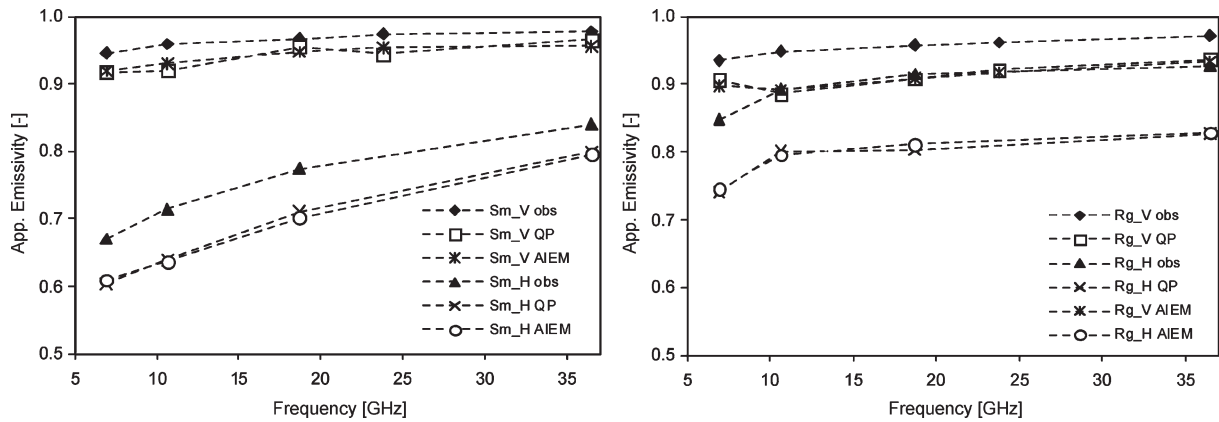Fig. 4.   Results of the QH simulation compared with observed data.

Fig. 5.   Results of AIEM and QP simulations compared with observed data.

emissions and a small reduction in vertically polarized emissions. This behavior is reproduced by both models; however, the absolute values of observed and simulated data contain discrepancies that cannot be ignored.

From the simulation results, it is evident that the QP model is indeed a parameterized version of AIEM; Fig. 6 shows this relationship succinctly. There is a 1 : 1 correspondence between the results of the two models for both polarizations. Vertically polarized emissivities show better agreement, with maximum differences within 0.01 ($\sim$2–3 K). Horizontally polarized emissions are in good agreement to within 0.02 ($\sim$4–6 K).

On the basis of these results, we conclude that the QP model can be used in place of AIEM within the limits of applicability of the QP model. This usage is subject to first clarifying the large discrepancy that is reported above.

To resolve the aforementioned discrepancy, we used only AIEM for further simulations. We undertook an analysis of the most significant contributions from a large array of settings within AIEM [using different Fresnel reflection formulations, considering backscatter enhancement (useful for active remote sensing), varying the surface correlation function, and including the effects of shadowing]. Incorporating the effects of shadowing was found to result in the most consistent simulation for a given soil state.

We now compare the results of using AIEM without shadowing (same as QP) with the results obtained using shadowing (with observed emissivities). The smooth case (Fig. 7, left)
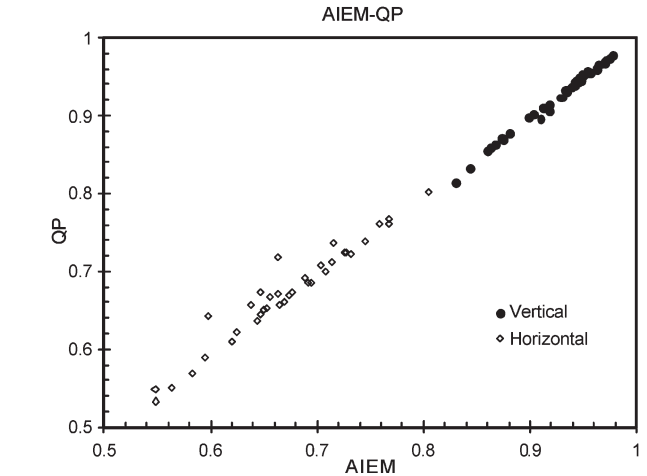

Fig. 6.   Relationship between AIEM and QP data.

represents the case where the surface is made as smooth as possible, whereas the rough case (Fig. 7, right) shows the results for a rough surface. In both cases, we note that when shadowing is not taken into account (original AIEM settings), the model results are underestimated. For the smooth case, there is good agreement between model results for which shadowing is taken into account and observed emissivities to within 0.01 ($\sim$3 K). In the rough case, the model (shadowing is taken into account) results are consistently slightly underestimated by $\sim$0.02
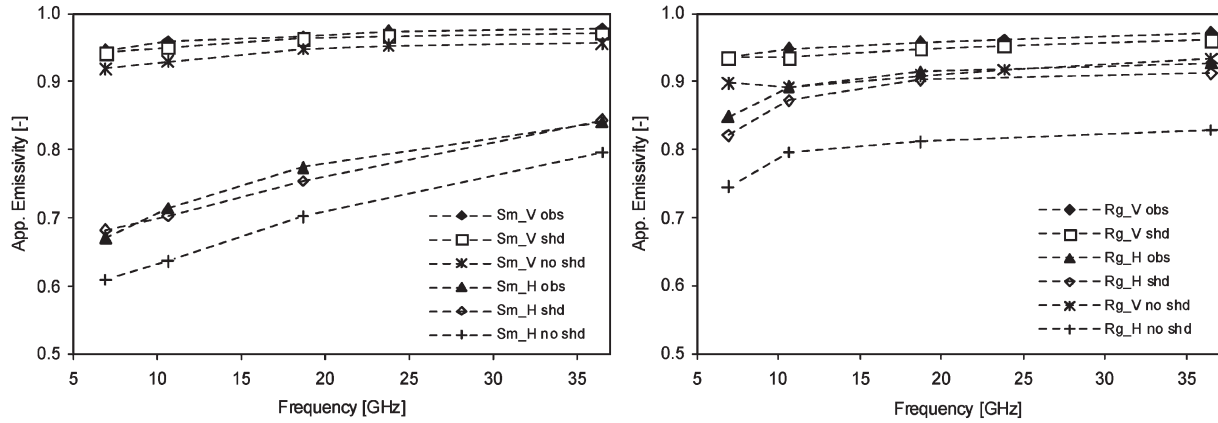
Fig. 7. Incorporating the effects of shadowing.

TABLE IV
VALUES USED TO GENERATE INPUT DATA FOR THE MODEL

T [K]	σ [cm]	ρ [cm]	ρ$_b$ [g/cm3]
278.842	0.35	0.5	1.67043

($\sim$6 K); this is apparently independent of polarization but is weakly dependent on frequency. Surprisingly, the smooth case contains a minor degree of roughness whose contribution to the shadowing effect is significant and therefore cannot be ignored.

B. Relationship Between Shadowing and Moisture

There are no data on the existence of a direct relationship between shadowing and moisture content; however, it is important to clarify if such a relationship exists because it is normally assumed that the effect of roughness (and now, shadowing) is enhanced by soil moisture. Such a relationship will provide insight into the possibility of incorporating shadowing into the QP model.

The data listed in Table IV were used to generate input data set for running the model. The model was first run without any consideration of shadowing effects and then run a second time while taking shadowing into account. The σ and ρ values were chosen from realistic roughness values for a natural terrain. Soil moisture was varied from 15% to 40%.

To investigate the relationship between moisture and shadowing, we determined the ratio of results derived from the shadowing case to those derived from the case in which shadowing was ignored. This ratio was then related to values of soil moisture on the basis that a constant value for the ratio would indicate a lack of any relationship. We found, however, that there is a relationship between the ratio and moisture (Fig. 8), and by extension, between the ratio and shadowing. The value of the ratio is also dependent on frequency and polarization. At lower values of moisture, the ratio is close to 1, and this value increases with increasing moisture content. For the horizontal case, we note that the effect is more pronounced at frequencies of 6.925 and 10.65 GHz than for other frequencies. For higher frequencies, the ratio is similar for both polarizations, with the value being slightly higher for horizontal cases.

Fig. 9 shows a linear relationship that is dependent on frequency and polarization. The 6.925- and 36.5-GHz cases

represent the general trends observed for all of the considered frequencies. In all cases, emissivity for shadowing case is higher than that for the no-shadowing case (the trend line is always above the dashed 1 : 1 line). In addition, the range of the relationship is dependent on frequency, as a wider range is observed for 6.925 GHz (0.55–1.0) than for 36.5 GHz (0.75–1.0). Considering the shadowing and no-shadowing cases, we note that the slopes of the vertical and horizontal polarization lines are similar for each frequency.

V. MODEL VALIDATION

To assess the performance of the model under natural conditions, we used the Coordinated Enhanced Observing Period (CEOP) Extended Observing Period phase 1 data. The period considered was January–August 2003. During this period, the following observations were made: soil moisture, soil temperature (each at both 3- and 10-cm depths), and AMSR brightness temperatures (6.925-, 10.65-, 18.7-, 23.8-, 36.5-, and 89-GHz dual polarization). In this paper, we present the results for site A3. In our validation, we do not include the 89-GHz data since we did not consider it during our experiment.

In Fig. 10, we show the results of our simulation against the observation. In this case, "AIEM" in the legend indicates AIEM considering shadowing.

On the assumption of temporal invariability of surface roughness condition, one best fitting surface roughness parameters set was used for the entire observation period. We have assumed that vegetation effects can be ignored since the target site is dry and vegetation free, and that the point data from the *in situ* site can be used to represent the satellite footprint's average surface condition. The data obtained when moisture condition was above 12% were used, since for moisture values lower than this, we would have volume scattering due to the deeper layers. Table V summarizes the parameters used for the simulation.

Fig. 10 is a representative of the analysis at all frequencies. From this figure, it is clear that AIEM incorporating shadowing demonstrates better agreement with observations than the QP model at all frequencies. Bearing in mind that QP is a parameterized version of AIEM, therefore, better simulation results would be expected when using QP model if shadowing effects were incorporated.
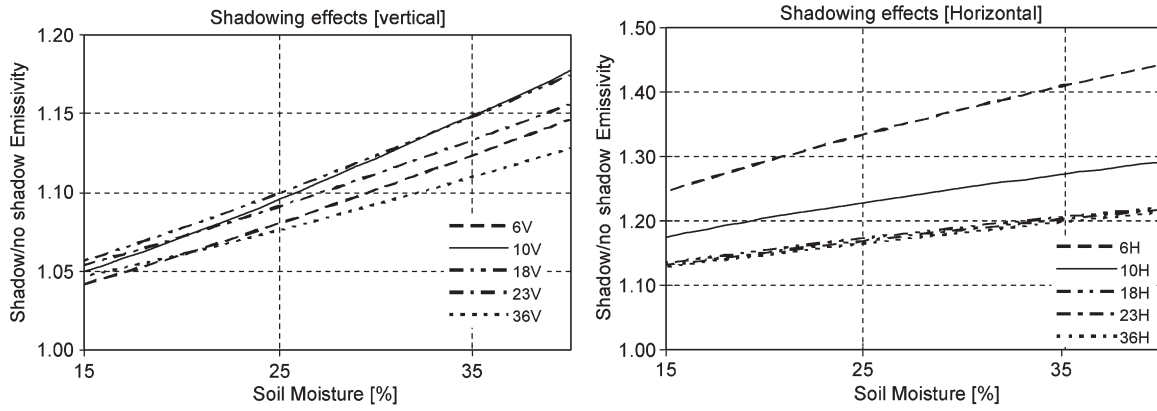
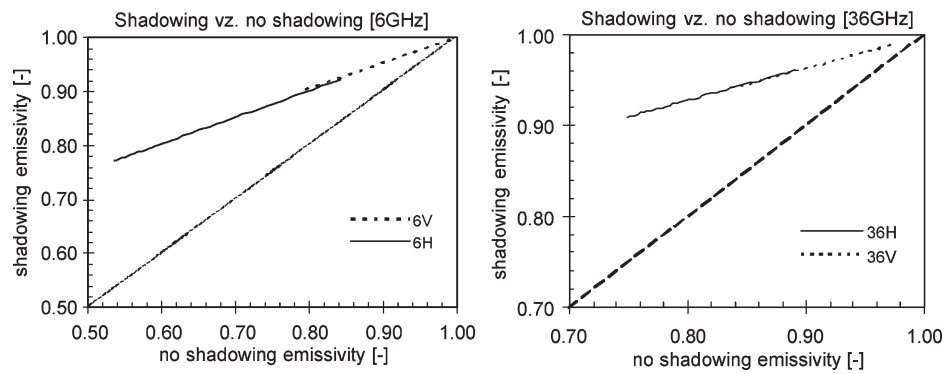Fig. 8.   Relationship between shadowing and moisture.

Fig. 9.   Comparison of model results (at 6.925- and 36.5-GHz frequencies) with and without shadowing being taken into account.
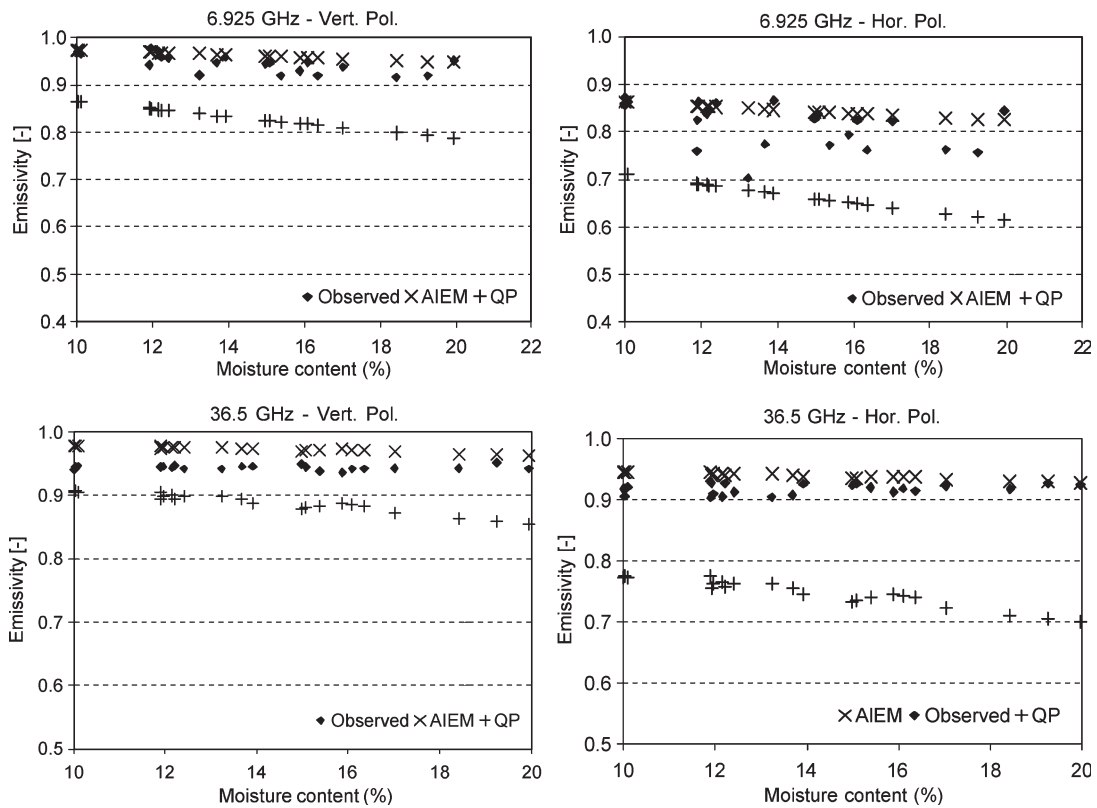

Fig. 10.   Mongolia site A3 simulated and observed emissivities.

TABLE V
MONGOLIA SITE A3 (CEOP) PARAMETERS

Parameter	Value(s)
Bulk density	1.256
Sand fraction	0.6
Clay fraction	0.2
r. m. s height (cm)	0.45
Correlation length (cm)	1.75

VI. CONCLUSION

The approaches we adopted in our experiment, such as using the AIEM, which was developed for modeling random rough surface emission, and using sand to model natural surface conditions, cause many shortcomings. However, when we compared the simulation at the CEOP Mongolia site A3 (which is a natural site and has a predominantly bare surface), we obtained better agreement between observed brightness temperatures and the simulated ones when we consider the effects of shadowing. In this case, we have assumed a transparent atmosphere at all frequencies. To minimize the effects of volume scattering, we restricted our analysis to data observed under soil moisture condition higher than 12%. For soil moisture less than 12%, it is necessary to consider volume scattering effects of the deeper layers.

On the basis of our field experiment, we verified that AIEM without taking shadowing into account is in good agreement with the QP models, as reported by the authors of the QP model. The two models agree to within 3 K for vertically polarized emissions and to within 6 K for horizontally polarized emissions; however, we have demonstrated that it is important to take shadowing into account if the surface emission model is to be of practical use in conjunction with AMSR-E data. The roughness parameters obtained from the experiment gives high values for random roughness slopes of 0.801 and 0.914 for the smooth and the rough surfaces, respectively. These values are rather high and justify our inclusion of the shadowing effects. Including shadowing effects in the general case therefore signals ability to transition from smooth surfaces to very rough surfaces easily.

Previous studies have reported that AIEM has a wide range of applicability from low to high frequencies. Our field experiment and model validation confirms that AIEM can be used to simulate surface emission reasonably well under wetter surface conditions. The simulation is significantly improved if the effects of shadowing are incorporated into the model. By taking into account the effects of shadowing, the model simulates observed values very well, with just a minor error ($\sim$2–6 K) that is largely independent of frequency.

Our study of the relationship between shadowing and moisture shows a positive relationship, with the effect of shadowing increasing with increasing moisture. This further reinforces the long-held notion that surface scattering effects dominate in the case of wet soil. Our comparison of the relationship between shadowing and no-shadowing results at different frequencies show that for a given roughness condition there exists a linear relationship whereby the slope is similar for both polarizations but the intercepts differ slightly. This signifies that the effect of shadowing can be parameterized. This finding is significant if the QP model is to be used because the QP model is in agreement with AIEM if shadowing effects are not taken into account. Parameterizing the shadowing effects would make it possible to use the QP model. This is especially significant because the major limitation of AIEM is the computational demands that it places on resources. These demands make it unsuitable to use AIEM in data-assimilation schemes, whereas the much simpler QP model does not make such demands.

In the past, retrievals of roughness and soil moisture were undertaken using vertical polarization because it was considered that horizontal polarization was subjected to some kind of instability. However, provided that the effects of shadowing are taken into account, both polarizations can be used in the retrieval. We have demonstrated that differences in the observed and simulated data appear to indicate polarization independence.

Due to the limitations in our field experiment setup, it is recommended that more field or laboratory experiments with truly random surfaces be conducted to conclusively validate the significance of the shadowing effect. We have used surfaces with high random slopes for our experiment and have assumed that volume scattering is insignificant at 15% moisture condition. Such future experiments should consider random surfaces with small random slopes and whether volume scattering can be ignored at intermediate moisture conditions as those considered in this paper.

REFERENCES

[1] N. C. Bruce, "On the validity of the inclusion of geometrical shadowing functions in the multiple scatter Kirchhoff approximation," *Waves Random Media*, vol. 14, no. 1, pp. 1–12, 2004.

[2] C. Bourlier, G. Berginc, and J. Saillard, "Monostatic and bistatic statistical shadowing functions from one-dimensional stationary randomly rough surface according to the observation length: I. Single scattering," *Waves Random Media*, vol. 12, no. 2, pp. 145–173, Apr. 2002.

[3] C. Bourlier and G. Berginc, "Shadowing function with single reflection from anisotropic Gaussian rough surface. Application to Gaussian, Lorentzian and sea correlations," *Waves Random Media*, vol. 13, no. 1, pp. 27–58, 2003.

[4] P. C. Y. Chang, J. C. Flitton, K. I. Hopcraft, E. Jakeman, D. Jordan, and J. G. Walker, "Importance of shadowing and multiple reflections in emission polarization," *Waves Random Media*, vol. 12, no. 1, pp. 1–19, Jan. 2001.

[5] K. Chen, T. D. Wu, L. Tsang, Q. Li, J. C. Shi, and A. K. Fung, "The emission of rough surfaces calculated by the integral equation method with a comparison to a three dimensional moment method simulation," *IEEE Trans. Geosci. Remote Sens.*, vol. 38, no. 1, pp. 249–256, Jan. 2001.

[6] B. J. Choudhury, T. J. Schmugge, A. Chang, and R. W. Newton, "Effect of surface roughness on the microwave emission from soil," *J. Geophys. Res.*, vol. 84, no. C9, pp. 5699–5706, 1979.

[7] M. C. Dobson, F. T. Ulaby, M. T. Hallikainen, and M. A. El-Rayes, "Microwave dielectric behavior of wet soil—Part II: Dielectric mixing models," *IEEE Trans. Geosci. Remote Sens.*, vol. GRS-23, no. 1, pp. 35–46, Jan. 1985.

[8] A. K. Fung, *Microwave Scattering and Emission Models and Their Applications*. Norwood, MA: Artech House, 1994.

[9] D. M. Milder, "Surface shadowing at small grazing angles," *Waves Random Media*, vol. 13, no. 2, pp. 89–94, 2003.

[10] T. Mo and T. J. Schmugge, "A parameterization of the effects of surface roughness on microwave emission," *IEEE Trans. Geosci. Remote Sens.*, vol. GRS-25, no. 1, pp. 47–54, Jan. 1987.

[11] E. G. Njoku, "AMSR land surface parameters," *Algorithm Theoretical Basis Document Version 3.0*, 1999.

[12] Y. Oh and C. K. Young, "Conditions for precise measurement of soil surface roughness," *IEEE Trans. Geosci. Remote Sens.*, vol. 36, no. 2, pp. 691–695, Feb. 1998.

[13] M. I. Sancer, "Shadow corrected electromagnetic scattering from randomly rough surfaces," *IEEE Trans. Antennas Propag.*, vol. AP-17, no. 5, pp. 577–585, Sep. 1969.

[14] D. Singh, K. P. Singh, I. Herlin, and S. K. Sharma, "Ground based scatterometer measurements of periodic surface roughness and correlation length for remote sensing," *Adv. Space Res.*, vol. 32, no. 11, pp. 2281–2286, 2003.

[15] J. C. Shi, L. Jiang, L. Zhang, K. S. Chen, J. P. Wigneron, and A. Chanzy, "A parameterized multifrequency-polarization surface emission model," *IEEE Trans. Geosci. Remote Sens.*, vol. 43, no. 12, pp. 2831–2841, Dec. 2005.

[16] B. G. Smith, "Geometrical shadowing of a random rough surface," *IEEE Trans. Antennas Propag.*, vol. AP-15, no. 5, pp. 668–671, Sep. 1967.

[17] L. Tsang, A. U. Kong, and R. T. Shin, *Theory of Microwave Remote Sensing*. New York: Wiley, 1985.

[18] F. T. Ulaby, R. K. Moore, and A. K. Fung, *Microwave Remote Sensing: Radar Remote Sensing and Surface Scattering and Emission Theory*, vol. 2. Norwood, MA: Artech House, 1982.

[19] F. T. Ulaby, R. K. Moore, and A. K. Fung, "Microwave backscatter dependence on surface roughness, soil moisture and soil texture fore bare soil," *IEEE Trans. Geosci. Remote Sens.*, vol. GRS-16, no. 4, pp. 286–295, Apr. 1986.

[20] J. R. Wang and B. J. Choudhury, "Remote sensing of soil moisture content over bare fields at 1.4 GHz frequency," *J. Geophys. Res.*, vol. 86, no. C6, pp. 5277–5282, Jun. 1981.

[21] J. R. Wang and T. J. Schmugge, "An empirical model for the complex dielectric permittivity of soils as a function of water content," *IEEE Trans. Geosci. Remote Sens.*, vol. GRS-18, no. 1, pp. 288–295, 1980.

[22] U. Wegmueller and C. Matzler, "Rough bare soil reflectivity model," *IEEE Trans. Geosci. Remote Sens.*, vol. 37, no. 5, pp. 1391–1395, May 1999.

[23] T. Wilheit, C. Kummerow, and R. Ferraro, "EOS/AMSR rainfall," *Algorithm Theoretical Basis Document*, 1999.

Toshio Koike received the B.Eng., M.Eng., and D.Eng. degrees from the University of Tokyo, Tokyo, Japan, in 1980, 1982, and 1985, respectively.

He was a Research Associate at the University of Tokyo in 1985 and was appointed as an Assistant Professor at the same university in 1986. He was also appointed as an Associate Professor at Nagaoka University of Technology, Nagaoka, Japan in 1992. He has been a Professor at the River and Environmental Engineering Laboratory, Department of Civil Engineering, University of Tokyo since 2000. He is the Lead Scientist of the Coordinated Enhanced Observing Period project. His research interests are in hydrology, water resources, satellite remote sensing, climate change, and Asian monsoons.

Hui Lu received the B.Eng. and M.Eng. degrees from Tsinghua University, Beijing, China, in 2000 and 2003, respectively, and the D.Eng. degree from the University of Tokyo, Tokyo, Japan, in 2006.

He is currently a Research Fellow with the River and Environmental Engineering Laboratory, Department of Civil Engineering, University of Tokyo. His research interests are radiative transfer model development through field experiments and numerical simulations, and passive microwave remote sensing of land surface parameters.

Hiroyuki Tsutsui received the B.Eng. and M.Eng. degrees from Nagaoka University, Niigata, Japan, in 1992 and 1994, respectively.

He is currently a Research Associate with the River and Environmental Engineering Laboratory, Department of Civil Engineering, University of Tokyo, Tokyo, Japan. His research interests include algorithm development for snow using passive microwave remote sensing.

David N. Kuria received the B.Sc. degree from the University of Nairobi, Nairobi, Kenya, in 1998, and the M.Sc. degree from the Stuttgart University of Applied Sciences, Stuttgart, Germany, in 2003. He is currently working toward the Ph.D. degree at the University of Tokyo, Tokyo, Japan.

His research interests are scattering of microwave and remote sensing of soil moisture and the atmosphere using multifrequency microwave.

Tobias Graf received the Dip.Ing. degree from the University of Stuttgart, Stuttgart, Germany in 2001 and the D.Eng. degree from the University of Tokyo, Tokyo, Japan in 2004.

He is currently a Research Associate with the River and Environmental Engineering Laboratory, Department of Civil Engineering, University of Tokyo. His research interests are snow modeling and passive microwave remote sensing of snow.